Positron trapping at grain boundaries

A. Dupasquier
Dipartimento di Fisica del Politecnico di Milano, Piazza Leonardo da Vinci 32, I-20133 Milano, Italy

R. Romero and A. Somoza
Instituto de Fisica de Materiales Tandil, Facultad de Ciencias Exactas,
Universidad Nacional del Centro de la Provincia de Buenos Aires, Pinto 399, 7000 Tandil, Argentina
(Received 31 March 1993)

The standard positron trapping model has often been applied, as a simple approximation, to the interpretation of positron lifetime spectra in situations of diffusion-controlled trapping. This paper shows that this approximation is not sufficiently accurate, and presents a model based on the correct solution of the diffusion equation, in the version appropriate for studying positron trapping at grain boundaries. The model is used for the analysis of new experimental data on positron lifetime spectra in a fine-grained Al-Ca-Zn alloy. Previous results on similar systems are also discussed and reinterpreted. The analysis yields effective diffusion coefficients not far from the values known for the base metals of the alloys.

I. INTRODUCTION

Positron trapping at lattice defects in solids is a well-known phenomenon, easily observed through marked effects on annihilation characteristics, which is at the basis of current techniques of defect detection (for general reviews, see Refs. 1 and 2). The trapping rate depends on different factors, related to the capture mechanism itself and to the transport of positrons from the point of thermalization to the vicinity of a trap. Transport factors are likely to be dominant when the transition rate from a free to a trapped state for a positron already present in the vicinity of a trap is so high that the stochastic positron density is depleted around the trap.[3–5] Considering that the diffusion approximation is in most cases adequate for a description of positron transport at thermal equilibrium,[6] the extreme situation where trapping is essentially controlled by transport factors has been called "diffusion-limited regime."[7] This is opposed to the other extreme, characterized by rapid transport and low transition rate, called "transition-limited regime," or "propagation regime" in order to stress the idea that positron motion in this case can be described as a Bloch wave propagation.[7] In practical situations, any intermediate case is of course possible.

The conditions leading from the propagation to the diffusion regime have been discussed by Hodges,[8] and all the mathematics one needs to describe capture in extreme or intermediate regimes has been elaborated by several authors.[3–5,9,10] Thus, the theoretical basis for interpreting positron annihilation measurements in most practical situations, and for designing experiments specifically aimed at measuring transport parameters, is now firmly established. We do not think, however, that this knowledge has always been used in the most effective way. Often the experimental data have not been interpreted using the rather cumbersome equations dictated by the diffusion model, but on the basis of simpler expressions which come from the standard trapping model (STM). The simplified STM treatment was indeed proposed by Brandt and Paulin[3] as an approximation "adequate in most cases" of diffusion-limited capture; in fact, it seriously underestimates the trapping probability.

We have gained our first-hand experience on the above problems with the analysis of new measurements of positron lifetime spectra in series of an Al-Ca-Zn alloy at different stages of grain growth. When comparing our results with previous studies, we have found many points of disagreement, arising from the different interpretation of the experimental data. Therefore, in the present paper we combine the presentation of our data with a review and a reinterpretation of the work of other authors.

The organization of this paper is as follows. Section II is intended to clarify where the interpretation of positron experiments based on STM equations is incorrect. In Sec. III we develop a model based on the diffusion equation for obtaining the expressions that link the parameters of positron lifetime spectra with the physical and geometrical variables controlling positron capture at grain boundaries. These expressions are then used in Sec. IV for the unified interpretation of all experimental results. We draw our conclusions in Sec. V. Details on experimental procedures are given in the Appendix.

II. THE BRANDT-PAULIN APPROXIMATION

The well-known positron trapping model[11–13] assumes that the number of positrons captured per unit time by a given species of traps is given by

$$T=\kappa N \ , \tag{1}$$

where N is the number of positrons present in the sample and κ is a time-independent parameter (*capture rate*) which depends on the nature and on the concentration of the traps. Equation (1) makes no allowance for a possible depletion of the stochastic positron density in the proximity of the traps, and therefore restricts the validity of the trapping model to the extreme transition-limited re-

gime. However, Brandt and Paulin suggested[3] extending the formal validity of the STM results even to the extreme diffusion-limited regime, on the basis of the following arguments.

(a) After a rapid transient, which most probably escapes observation with any practical setup, the lifetime spectrum is approximately formed by two components only, as predicted by the STM (we consider here the case of a single trap species).

(b) The decay rates of the above components are given by the following expressions, formally identical to STM formulas:

$$\lambda_A = \lambda_{\text{bulk}} + \kappa^* \tag{2}$$

and

$$\lambda_B = \lambda_{\text{trap}} , \tag{3}$$

where λ_{bulk} is the bulk annihilation rate for free positrons, λ_{trap} is the annihilation rate for trapped positrons, and κ^* is an effective capture rate, related to geometrical factors and to the positron diffusion constant D_+; for trapping at the surface of a spherical domain of radius R, one has

$$\kappa^* = \pi^2 \frac{D_+}{R^2} . \tag{4}$$

(c) The intensity of the long-living component I_B is approximately related to the effective capture rate by the familiar STM expression

$$I_B = \frac{\kappa^*}{\lambda_{\text{bulk}} + \kappa^* - \lambda_{\text{trap}}} . \tag{5}$$

We agree that (a) is a reasonable assumption, and that (b) is the mathematically correct result in the extreme diffusion-limited regime (we shall return to this point in the following section; however, see also Ref. 4). On the contrary, we must disagree with (c), since Eq. (5) is a bad underestimate of the "exact" result coming from the diffusion model. The entity of the discrepancy is well above the error limits (1–2 %) that can be reached with modern experimental techniques; this can be verified at first sight in the example shown in Fig. 1, where curve (a) is the exact result, identical to curve 3 in Fig. 1 of Ref. 3, valid for the extreme diffusion-limited regime in spherical symmetry and for $\lambda_{\text{trap}} \ll \lambda_{\text{bulk}}$, and curve (b) is calculated from Eq. (5), which comes from Eq. (19) of Ref. 3.

Unfortunately, the Brandt-Paulin approximation has been accepted without objections for 20 yr. The consequences are serious. Many evaluations of positron transport parameters, based on trapping phenomena, need to be corrected. Many physical hypotheses, made in order to explain the clear disagreement between good experimental data and poor theory, need to be reconsidered. In view of the revision work awaiting us, it is convenient to point out that: (a) the approximated evaluation of the positron diffusion constant from lifetime data on the basis of Eqs. (2) and (4) (or of similar equations, valid for different geometries) is theoretically correct; however, as the results presented in Sec. IV will show, the systematic

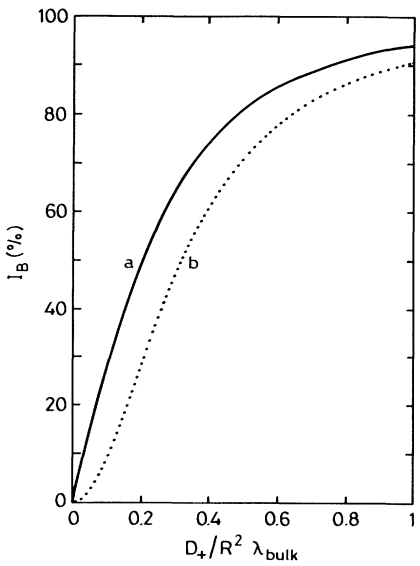

FIG. 1. I_B vs $D_+/(\lambda_{\text{bulk}}R^2)$ in the extreme diffusion-limited regime. Curve a is the result of the exact diffusion model and curve b is the Brandt-Paulin approximation; both curves are calculated for spherical symmetry and for $\lambda_{\text{trap}} \ll \lambda_{\text{bulk}}$.

dependence of λ_A on R and D_+ predicted by the theory is often of the same order of magnitude as the statistical dispersion of the experimental points; therefore, the precision of a D_+ estimate based exclusively on lifetime data can only be poor; (b) since Eq. (5) is a poor approximation, the following STM relationships, currently used for interpreting lifetime data, should never be adopted when positron capture is influenced, at any level, by transport factors:

$$\lambda_A = \lambda_{\text{bulk}} + (\lambda_{\text{bulk}} - \lambda_{\text{trap}}) \frac{I_B}{I_A} , \tag{6}$$

$$\lambda_{\text{bulk}} = I_A \lambda_A + I_B \lambda_B , \tag{7}$$

$$\kappa^* = (\lambda_{\text{bulk}} - \lambda_{\text{trap}}) \frac{I_B}{I_A} , \tag{8}$$

$$\kappa^* = \lambda_{\text{bulk}} \frac{\bar{\tau} - \tau_{\text{bulk}}}{\tau_{\text{trap}} - \bar{\tau}} ; \tag{9}$$

in the latter equation, $\tau_{\text{bulk}} = 1/\lambda_{\text{bulk}}$, $\tau_{\text{trap}} = 1/\lambda_{\text{trap}}$, and $\bar{\tau} = I_A/\lambda_A + I_B/\lambda_B$; also remember that we have assumed $\lambda_B = \lambda_{\text{trap}}$.

III. DIFFUSION TRAPPING MODEL

The discussion in the previous section leads to the conclusion that the full formalism which derives from the integration of the diffusion equation cannot be avoided. We develop here a model of positron trapping based on the diffusion equation (henceforth called "diffusion trapping model" or, in brief, DTM) in a version appropriate for trapping at grain boundaries, under the following simplifying assumptions: (a) the material is formed by identical spherical domains of radius R; (b) positron trapping

occurs only at the surface of the domains, in a disordered region of constant thickness $\delta \ll R$; (c) the thermal trapping rate κ_s in this disordered region is much larger than the local annihilation rate of free positrons; on the contrary, prethermalization trapping is negligible; (d) detrapping is also negligible; (e) all trapped positrons annihilate with the same rate λ_{trap}.

According to the above assumptions, the number of positrons getting trapped at the surface of a domain in unit time is

$$T = \kappa_s 4\pi R^2 \delta \cdot n_R \ , \tag{10}$$

where n_R is the stochastic free positron density $n(r,t)$ evaluated at the surface of the domain, i.e., for $r=R$. The assumption $\delta \ll R$ enables us to neglect the fraction of positrons that completes the thermalization inside the surface layer, and to set T equal to the density gradient-driven current passing through the interface between the ordered region inside the domain and the disordered surface layer. We thus write

$$T = -4\pi R^2 D_+ \left[\frac{\partial n}{\partial r} \right]_{r=R} . \tag{11}$$

By combining Eqs. (10) and (11) one obtains

$$\left[\frac{\partial n}{\partial r} \right]_{r=R} = -\frac{\kappa_s \delta}{D_+} n_R \ , \tag{12}$$

which is the boundary condition for the diffusion equation governing the space and time dependence of the positron density $n(r,t)$:

$$\frac{\partial n}{\partial t} = D_+ \left[\frac{\partial^2 n}{\partial r^2} + \frac{2}{r} \frac{\partial n}{\partial r} \right] - \lambda_{\text{bulk}} n \ . \tag{13}$$

The solution of this equation can be found in standard textbooks (see, for instance, Ref. 14) if Eq. (12) is rewritten in the form

$$\left[\frac{\partial n}{\partial r} \right]_{r=R} = -\frac{\alpha}{R} n_R \ . \tag{14}$$

Taken together, Eqs. (12) and (14) define a *regime parameter* α, which characterizes the balance between capture-limiting factors. The limit $\alpha \to \infty$ corresponds to the extreme diffusion-limited regime; at the other extreme, $\alpha = 0$ gives the uniform free positron density expected for transition-limited capture. A convenient way of expressing α in terms of the key variables of the problem is

$$\alpha = \frac{\kappa_s}{\lambda_{\text{bulk}}} \frac{\delta}{L_+} \frac{R}{L_+} \ , \tag{15}$$

where L_+ is the positron diffusion length $\sqrt{D_+ / \lambda_{\text{bulk}}}$ (note that some authors include a numerical factor in their definition of the diffusion length).

In Ref. 3, where only the extreme diffusion-limited regime was considered, a corresponding expression of a "regime parameter" is not given. We stress, however, that the correct dependence of α on R is essential for studying the effect of changing disorder density on positron capture (the trapping surface per unit volume σ is related to R by the equation $\sigma = 3/R$). A connection between the capture regime and a geometrical variable related to the defect density is also to be found in other situations of positron trapping; examples, regarding trapping at dislocations and voids, are in Refs. 9 and 10. Hodge's statement[8] that the capture regime "has nothing to do with defect separation" is not supported by a complete analysis, without restrictions to limit cases.

The analytical solution of Eqs. (13) and (14), including the initial condition

$$n(r,0) = \left[\frac{4}{3} \pi R^3 \right]^{-1} \tag{16}$$

(one positron per domain), is

$$n(r,t) = \left[\frac{4}{3} \pi R^3 \right]^{-1} \frac{R}{r} \times \sum_{n=1,\infty} a_n \exp(-\lambda_n t) \frac{\sin(\beta_n r/R)}{\sin \beta_n} \ , \tag{17}$$

where β_n is the nth solution of the eigenvalue equation

$$\beta_n \cot \beta_n + \alpha - 1 = 0 \ , \tag{18}$$

$$a_n = \frac{2\alpha}{\beta_n^2 + \alpha(\alpha - 1)} \ , \tag{19}$$

$$\lambda_n = \lambda_{\text{bulk}} (1 + \beta_n^2 L_+^2 / R^2) \ . \tag{20}$$

By combining Eq. (17) with Eq. (10) or, equivalently, with Eq. (11), one obtains

$$T = \frac{3\kappa_s \delta}{R} \sum_{n=1,\infty} a_n \exp(-\lambda_n t) \ . \tag{21}$$

This expression can be used as a source term in the rate equation describing the time evolution of the number N_s of positrons trapped in the surface layer:

$$\frac{dN_s}{dt} = -\lambda_{\text{trap}} N_s + T \ , \tag{22}$$

to be solved with the initial condition $N_s(0) = 0$. The number N_f of free positrons can be obtained, indifferently, by spatial integration of the density $n(r,t)$ or by integrating the rate equation

$$\frac{dN_f}{dt}=-\lambda_{\text{bulk}}N_f-T\ , \tag{23}$$

with the initial condition $N_f(0)=1$.

We remark that Eqs. (22) and (23), with the correct expression [Eq. (21)] for T instead of the STM approximation [Eq. (1)], represent the generalization of the trapping model for any capture regime (any α), and are the key equations of what we have called the diffusion trapping model.

The final results for N_f and N_s are

$$N_f=3\alpha\left[\frac{L_+}{R}\right]^2\sum_{n=1,\infty}\frac{\lambda_{\text{bulk}}}{\lambda_n-\lambda_{\text{bulk}}}a_n e^{-\lambda_n t}\ , \tag{24}$$

$$N_s=3\alpha\left[\frac{L_+}{R}\right]^2\sum_{n=1,\infty}\frac{\lambda_{\text{bulk}}}{\lambda_n-\lambda_{\text{trap}}}a_n(e^{-\lambda_{\text{trap}}t}-e^{-\lambda_n t})\ . \tag{25}$$

Hence the lifetime spectrum $S(t)=\lambda_{\text{bulk}}N_f+\lambda_{\text{trap}}N_s$ takes the form

$$S(t)=3\alpha\left[\frac{L_+}{R}\right]^2\lambda_{\text{bulk}}\sum_{n=1,\infty}a_n\left[\frac{\lambda_{\text{bulk}}}{\lambda_n-\lambda_{\text{bulk}}}-\frac{\lambda_{\text{trap}}}{\lambda_n-\lambda_{\text{trap}}}\right]e^{-\lambda_n t}+3\alpha\left[\frac{L_+}{R}\right]^2\lambda_{\text{bulk}}\left[\sum_{n=1,\infty}a_n\frac{\lambda_{\text{trap}}}{\lambda_n-\lambda_{\text{trap}}}\right]e^{-\lambda_{\text{trap}}t}\ . \tag{26}$$

As pointed out by Brandt and Paulin (and by many other authors), the infinitely many components of $S(t)$ cannot be resolved in any practical experimental situation. If the data are analyzed using a two-component scheme, according to the equation

$$S(t)=\lambda_A I_A e^{-\lambda_A t}+\lambda_B I_B e^{-\lambda_B t}\ , \tag{27}$$

most probably only the long-living component will be isolated with accurate values for the decay rate $\lambda_B=\lambda_{\text{trap}}$ and for the intensity

$$I_B=3\alpha\left[\frac{L_+}{R}\right]^2\sum_{n=1,\infty}c_n\ , \tag{28}$$

where $c_n=a_n\lambda_{\text{bulk}}/(\lambda_n-\lambda_{\text{trap}})$. In the transition-limited regime (small α), only the first term of the infinite sum in Eq. (28) is important. Using the relationships

$$\lim_{\alpha\to 0}\beta_1^2/\alpha=3\ , \tag{29}$$

$$\lim_{\alpha\to 0}a_1=1\ , \tag{30}$$

$$\lim_{\alpha\to 0}a_{n>1}=0\ , \tag{31}$$

one retrieves from Eq. (28) the STM result

$$I_B=\frac{\kappa}{\lambda_{\text{bulk}}+\kappa-\lambda_{\text{trap}}}\ , \tag{32}$$

where the new parameter

$$\kappa=3\kappa_s\delta/R \tag{33}$$

can be interpreted as the product of a specific trapping rate $\nu=\kappa_s\delta$ times the specific surface $\sigma=3/R$.

We emphasize that, except for the case $\alpha\to 0$, the truncation of the sum in Eq. (28) to the first or to the few first terms might be quite inaccurate. In the most unfavorable case (large α and $R\gg L_+$), the truncation at $n=\alpha$ gives an inaccuracy $\Delta I_B/I_B\approx 10\%$; however, for finite values of the ratio R/L_+ the convergence is more rapid, so that in practice the truncation at $n\geq\alpha$ turns out to be always acceptable. For better orientation on this point, the ratio c_n/c_1 is plotted vs n in Fig. 2 for a few typical cases. The numerical evaluations of I_B presented in the following section were obtained by a personal computer routine that increases the number of terms included in the sum from a minimum of 10 to a maximum of 2000, which is reached for the largest α ($\alpha_{\max}=2000$) included in our calculation.

The results that one obtains for the short-living part of the spectrum, compressed into component A by the approximated two-term fit, depend on the resolution of the experimental setup and on other constraints of the analysis. The normalization constraint $I_A=1-I_B$ assigns the total intensity of the fast-decaying components to component A. However, since measurement and analysis procedures always privilege slower terms, the apparent decay rate will not be far from

$$\lambda_A\approx\lambda_1=\lambda_{\text{bulk}}\left[1+\beta_1^2\left[\frac{L_+}{R}\right]^2\right]\ . \tag{34}$$

Equation (34), with the approximation $\beta_1\approx\pi$ holding for large α, justifies the Brandt-Paulin equations (2) and (4).

The combination of Eqs. (28) and (34) implies an approximated correlation between λ_A and I_B, which substitutes Eq. (6). As an example, in Fig. 3 we have plotted $\lambda_A/\lambda_{\text{bulk}}$ vs $I_B/(1-I_B)$ as obtained from Eqs. (28) and (34) for variable R/L_+ and for fixed values of the other

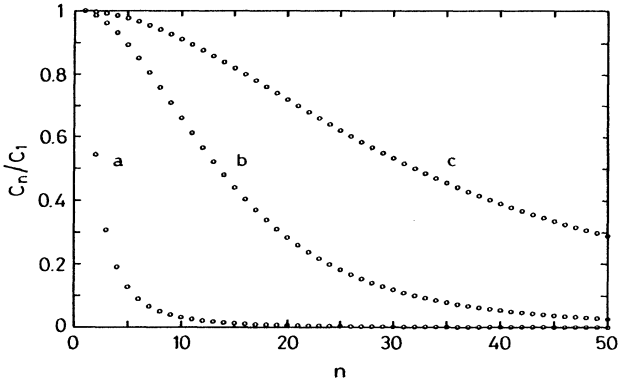

FIG. 2. Ratio c_n/c_1 vs n for $\alpha=100$, $\lambda_{\text{trap}}=0.75\lambda_{\text{bulk}}$, $R=10L_+$ (curve a), $R=100L_+$ (curve b), and $R=\infty$ (curve c).

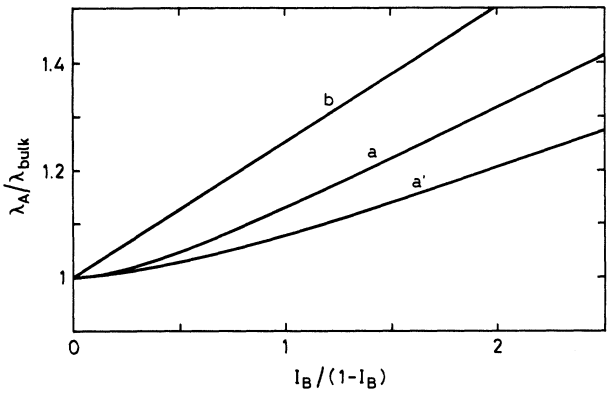

FIG. 3. Model predictions for the dependence of the decay rate λ_A on the intensity I_B for $\lambda_{trap}=0.75\lambda_{bulk}$, $\nu=5\lambda_{bulk}L_+$ and variable R: curve a is the plot of λ_A/λ_{bulk} vs $I_B/(1-I_B)$ as predicted by the DTM; curve a' is also a DTM result, but includes the radius correction discussed in the text; line b is the STM prediction.

parameters ($\lambda_{trap}/\lambda_{bulk}=0.75$ and $\nu/\lambda_{bulk}L_+=5$). The figure also shows the STM straight line, Eq. (6). This comparison shows that the slope of the DTM curve is always less than the one predicted by the STM. Actually, even less slope is to be expected for a sample containing grains of different sizes, a case not considered in the present DTM version but certainly occurring in any real experiment; the reason is that the apparent decay rate λ_A will probably approach the λ_1 value corresponding to the largest grains, while the dominant contributions to I_B come from the smallest grains. Curve a' in Fig. 3 is obtained by assuming the existence of a distribution of radii with a dispersion above 20%, and by taking for Eq. (28) a radius 10% below the average and for Eq. (34) a radius 10% above the average.

IV. EXPERIMENTAL RESULTS

In this section, experimental results regarding positron lifetime spectra in fine-grained alloys are interpreted or reinterpreted on the basis of DTM equations. The discussion includes our results as well as those of other authors, and is extended to a variety of Al-, Zn-, and Fe-based alloys. Full details on our measurement and analysis procedures are given in the Appendix; for the procedures followed in other laboratories, the reader is referred to the original publications (references below).

A. Al-based alloys

Existing data concern Al-5 wt % Ca-5 wt % Zn (this work and Ref. 15; de Diego and Hidalgo[16]), Al-6 wt % Ni (McKee *et al.*[17]) and Al-6 wt % Ni-0.3 wt % Mg (McKee *et al.*[17]). There are differences between the cited works in the thermal treatments adopted in order to obtain grain coarsening, but this seems to be irrelevant to the final correlation between grain size and positron lifetime parameters; we have specifically ascertained this point by studying separately three series of samples isothermally annealed at three different temperatures (773 K, 798 K, and 863 K).

For the above systems, the two-component analysis of the spectra gives qualitatively similar results: the decay rate of the long-living component λ_B is not correlated to the grain size, the fast decay rate λ_A and the intensity of the long-living component I_B both decrease for increasing grain sizes, and therefore are positively intercorrelated; this correlation, however, is not that predicted by the STM. The quantitative comparison of the results is possible after correcting for the contribution to trapping of second-phase particles (intermetallic compound precipitates). Indeed, apart from precipitate effects, the different composition of the alloys is not a very important factor, because the segregation of insoluble minority elements in the form of intermetallic compounds leaves an Al matrix with a small amount of substitutional impurities in ca. 80% of the sample volume.

The correction for the effect of the precipitates is a delicate point. A contribution to the intensity of the long-living component certainly comes from trapping at the matrix-precipitate interface. A further contribution might come from a volume effect, due to trapping at pointlike defects frozen inside the precipitates. Volume trapping has indeed been invoked[18] for explaining the discrepancy between experimental results and STM predictions. Since we are now free from this preoccupation, we disregard the possibility of volume effects, and correct the experimental data only for the interface contribution, as explained below. Indeed, the hypothesis of trapping at the matrix-precipitate interface is in agreement with the result that the lifetime of the long-living component is unaffected by the microstructure of the sample. Interfaces of different size and shape probably appear more or less identical to positrons, which, after trapping, probe the local disorder at an atomic scale.

In order to account for the contribution of the precipitates to the intensity of the long-living component, we assume that trapping at matrix-precipitate interfaces occurs by the same mechanism as that controlling capture at grain boundaries. Thus, if the positron diffusion constants in the Al matrix and in the precipitate are not too different, the correction of the experimental data can be limited to a readjustment of the geometrical scale, in order to account for the different average dimensions of the precipitates and of the matrix grains. In Al-5 wt % Ca-5 wt % Zn the second-phase particles are $CaZnAl_3$ spheroidal precipitates, uniformly dispersed in the Al matrix. The thermal treatment producing grain coarsening also results in the growth of the precipitates; however, the average size ratio and the volume fractions of the two phases are substantially unaffected by thermal treatments. Using the experimental value 0.75 for the precipitate-grain size ratio, and the equilibrium value 0.2 for the volume fraction of the $CaZnAl_3$ phase, we relate the overall average radius to the measured grain size d by the equation $R=0.91d/2$. We have thus adopted this size rescaling for our data as well as for those of Ref. 16, which concern the same material. The situation for Al-6 wt % Ni and Al-6 wt % Ni-0.3 wt % Mg is, however, different, because the dimensions of second-phase parti-

cles ($NiAl_3$ precipitates) are not modified by thermal treatments, even after complete recrystallization of the matrix. It is therefore easier, and probably more accurate, to correct decay rates and intensities by subtracting the precipitate contribution, rather than alter the geometrical scale of the domains. We have done so in an approximated way, with the help of the following equations derived from the STM:

$$\lambda_A = \lambda_A^* - (\lambda_A^\infty - \lambda_{\text{bulk}}) , \tag{35}$$

where λ_A is the corrected rate, λ_A^* is the measured rate, λ_A^∞ is the rate measured after recrystallization, and λ_{bulk} is the rate expected for the matrix material

$$I_B = \left[\frac{I_B^*}{1-I_B^*} - \frac{I_B^\infty}{1-I_B^\infty} \right] \Big/ \left[1 + \frac{I_B^*}{1-I_B^*} - \frac{I_B^\infty}{1-I_B^\infty} \right] , \tag{36}$$

where I_B is the corrected intensity, I_B^* is the measured intensity, and I_B^∞ is the residual intensity after recrystallization (19%). The entity of the corrections is $<6\times10^{-4}$ ps^{-1} for decay rates and from 8 to 16 % for intensities.

The above corrections enable us to accommodate all experimental data in a series of unified plots, and to draw overall best-fit DTM curves. Figures 4 and 5 show, respectively, the intensity I_B and the decay rate ratio $\lambda_A/\lambda_{\text{bulk}}$ versus the average domain radius R. For λ_{bulk} we have taken the reciprocal of the lifetime measured for pure Al (a different value for each set of experimental data: 158 ps, Ref. 17; 161 ps, Ref. 16; 164 ps, this work; the average of the above values for DTM calculations). Independent fits of DTM curves [Eqs. (28) and (34)] to intensity and decay rate data, using as free parameters the diffusion length L_+ and the ratio of the specific capture rate $\nu=\kappa_s\delta$ to the bulk annihilation rate λ_{bulk}, reproduce the experimental behaviors very well, but lead to different values of the best-fit parameters. More specifically, we obtain acceptable fits of the intensity data only with diffusion lengths above 110 nm, while decay rate data cannot be fitted with L_+ above 90 nm. We believe that the discrepancy does not come from experimental errors but from the difference in the effective radii (indicated below as R' and R'') that are to be used in Eqs. (28) and (34). It is indeed possible to reconcile the fittings of both sets of data by taking into account a radius correction of the order of the statistical dispersion of the domain sizes, in the direction suggested by the discussion at the end of the previous section ($R'<R<R''$). The curves shown in Figs. 4 and 5 were obtained by taking $R'=(1-\varepsilon)R$ and $R''=(1+\varepsilon)R$, with ε fixed at the minimum value (0.12) allowing us to obtain consistent fittings of decay rate and intensity data; the ratio $\lambda_{\text{trap}}/\lambda_{\text{bulk}}$ was fixed as the mean of the values obtained in the different experiments (0.68). The values of the best-fit parameters are $L_+=95$ nm and $\nu/\lambda_{\text{bulk}}=500$ nm. In the explored radius interval, $\alpha>24$; this means that we are not too far from the extreme diffusion-limited regime, and that the fitting is much more affected by L_+ than by $\nu/\lambda_{\text{bulk}}$. Therefore, the indetermination interval of L_+ is relatively narrow (of the order of 5%), whereas $\nu/\lambda_{\text{bulk}}$ is essentially limited only at the low extreme (ca. 400 nm). In a preliminary report[15] we quoted 120 nm as our best estimate of L_+; this value was obtained without taking into account decay rate data and radius corrections, and also by using the constraint $\kappa=3\nu/R=$const, which is a less realistic assumption than $\nu=$const.

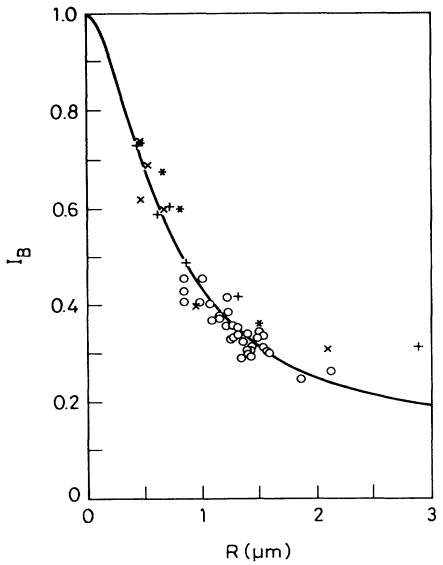

FIG. 4. Intensity of the long-living component vs mean domain radius in Al-based alloys. Experimental points: ○: Al-5 wt % Ca-5 wt % Zn, this work; ⁎: Al-5 wt % Ca-5 wt % Zn, Ref. 16; ×: Al-6 wt % Ni, Ref. 17; +: Al-6 wt % Ni-0.3 wt % Mg, Ref. 17. Theoretical curve: combined DTM best-fit of intensity and decay rate data.

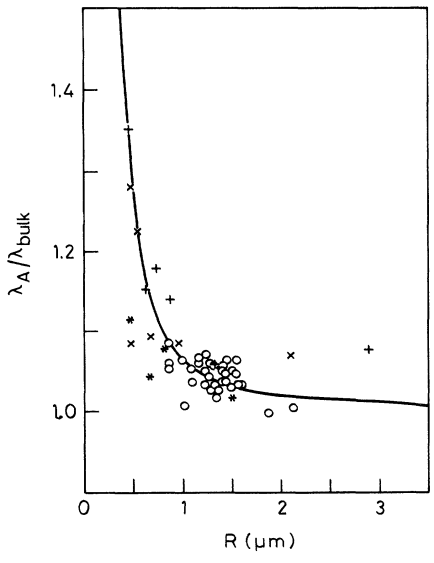

FIG. 5. Fast decay rate λ_A vs mean domain radius in Al-based alloys. Experimental points: ○: Al-5 wt % Ca-5 wt % Zn, this work; ⁎: Al-5 wt % Ca-5 wt % Zn, Ref. 16; ×: Al-6 wt % Ni, Ref. 17; +: Al-6 wt % Ni-0.3 wt % Mg, Ref. 17. Theoretical curve: combined DTM best fit of intensity and decay rate data.

It is instructive to see how the rate-intensity correlation predicted by the DTM fits the experimental data much better than the STM prediction. We have thus plotted the ratio $\lambda_A/\lambda_{\text{bulk}}$ against $I_B/(1-I_B)$ in Fig. 6; the DTM curve corresponds to the best-fit curves shown in Figs. 4 and 5, and the straight line is the STM prediction [Eq. (6)].

The experimental determination of the mean life $\bar{\tau}$ is, in most cases, more accurate than that of other characteristics, due to internal error compensations between lifetimes and intensities. For this reason, many discussions of experimental data are essentially based on $\bar{\tau}$ variations. In our case, having already determined the best-fit parameters using intensity and decay rates, an independent fitting of $\bar{\tau}$ is unnecessary. We thus show the plot of the ratio $\bar{\tau}/\tau_{\text{bulk}}$ (mean life over bulk lifetime) versus R in Fig. 7, with the DTM curve calculated with the values of the best-fit parameters listed above. The experimental points include the corrections already discussed, beside an offset to the lifetimes of the long-living component as needed for reconciling the values obtained in the four different experiments.

B. Zn-based alloys

The largest collection of room-temperature data, taken for different grain sizes, is for Zn-22 wt % Al (McKee *et al.*[19] and Dong, Xiong, and Lung[20]); two points for Zn-0.123 wt % Al-0.063 wt % Mg with a fine-grained structure are also given by Hidalgo *et al.*,[21] in a study concerning temperature effects on trapping at grain boundaries.

We report in Figs. 8 and 9 the plots of I_B and of λ_A vs

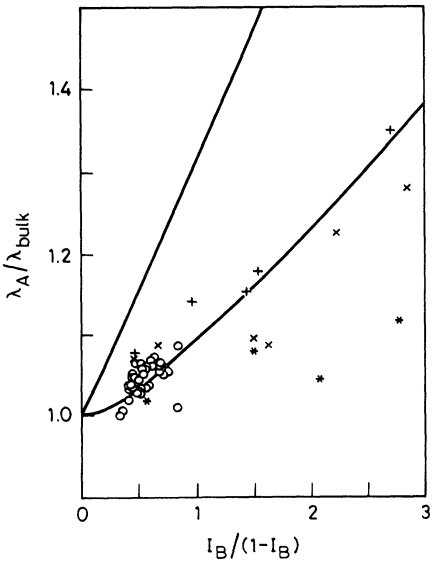

FIG. 6. Fast decay rate λ_A vs $I_B/(1-I_B)$ in Al-based alloys. Experimental points: ○: Al-5 wt % Ca-5 wt % Zn, this work; ⁎: Al-5 wt % Ca-5 wt % Zn, Ref. 16; ×: Al-6 wt % Ni, Ref. 17, +: Al-6 wt % Ni-0.3 wt % Mg, Ref. 17. The curve is the DTM result, corresponding to the best-fit curves of Figs. 4 and 5. The straight line is the STM prediction.

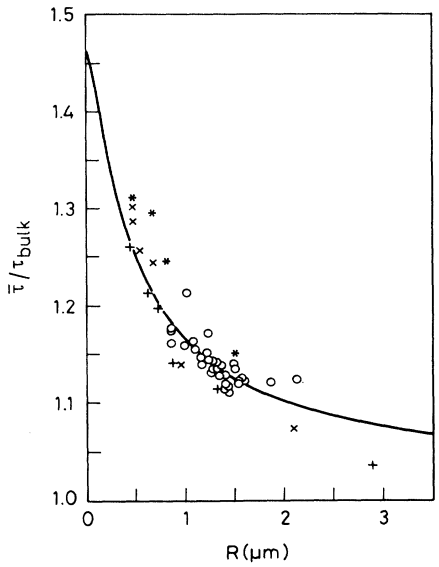

FIG. 7. Mean life $\bar{\tau}$ vs mean domain radius in Al-based alloys. Experimental points: ○: Al-5 wt % Ca-5 wt % Zn, this work; ⁎: Al-5 wt % Ca-5 wt % Zn, Ref. 16; ×: Al-6 wt % Ni, Ref. 17; +: Al-6 wt % Ni-0.3 wt % Mg, Ref. 17. The curve is the DTM result, corresponding to the best-fit curves shown in Figs. 4 and 5.

R, including all experimental data. We have not corrected the data of Refs. 19 and 20 for the contribution of the precipitates to positron trapping, which, according to Ref. 19, should be negligible. We remark, however, that the observed persistence of intense positron trapping even with large grain sizes is not easily explained without calling in question the effect of the precipitates. On the

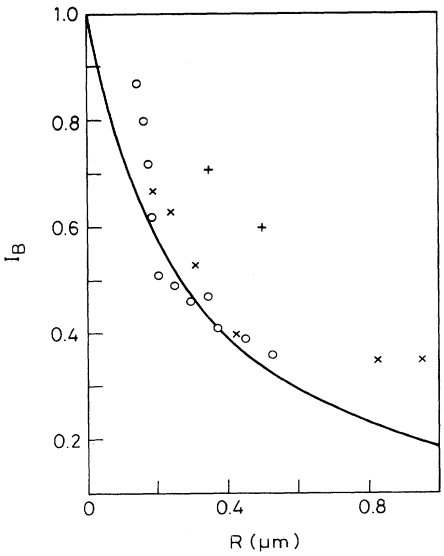

FIG. 8. Intensity of the long-living component vs mean domain radius in Zn-based alloys. Experimental points: ×: Zn-22 wt % Al, Ref. 19; ○: Zn-22% Al, Ref. 20; +: Zn-0.123 wt % Al-0.063 wt % Mg, Ref. 21. Theoretical curve: combined DTM best fit of intensity and decay rate data.

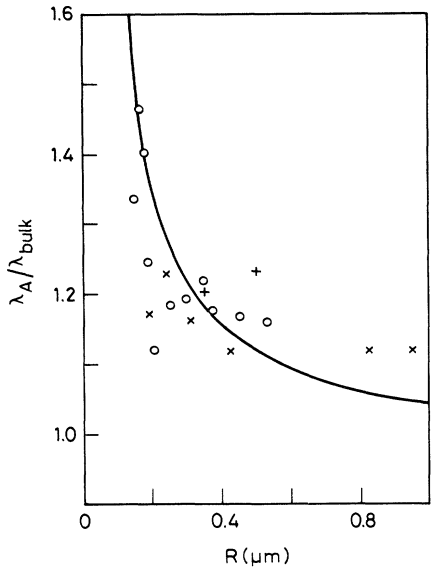

FIG. 9. Fast decay rate λ_A vs mean domain radius in Zn-based alloys. Experimental points: ×: Zn-22 wt % Al, Ref. 19; ○: Zn-22% Al, Ref. 20; +: Zn-0.123 wt % Al-0.063 wt % Mg, Ref. 21. Theoretical curve: combined DTM best fit of intensity and decay rate data.

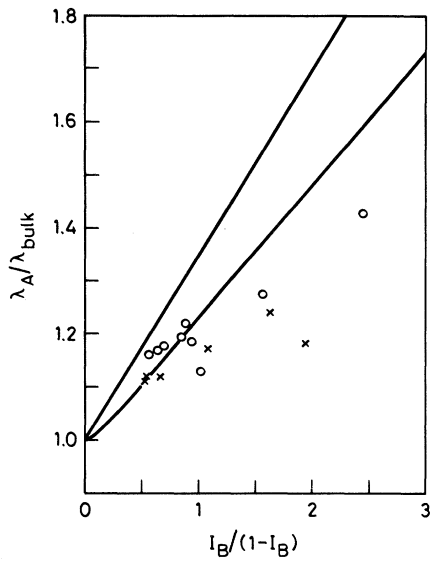

FIG. 10. Fast decay rate λ_A vs $I_B/(1-I_B)$ in Zn-based alloys. Experimental points: ×: Zn-22 wt % Al, Ref. 19; ○: Zn-22% Al, Ref. 20. The curve is the DTM result, corresponding to the best-fit curves of Figs. 8 and 9. The straight line is the STM prediction.

other hand, corrections are certainly needed for the data concerning Zn-0.123 wt % Al-0.063 wt % Mg, since the effect of the precipitates is evident in this case.[21,22] Unfortunately, discounting intensities and decay rates as dictated by Eqs. (35) and (36) does not seem sufficient to render compatible the results obtained for the two different alloys; therefore, the data of Ref. 21, although included in Figs. 8 and 9 with the mentioned corrections, were disregarded for the best fitting. The DTM curves shown in these figures correspond to $\varepsilon=0.12$ (chosen with the same criterion adopted for Al alloys), $\lambda_{bulk}=(160\ \text{ps})^{-1}$; $\lambda_{trap}=(245\ \text{ps})^{-1}$, and to the following values of the best-fit parameters: $L_+=100$ nm and $\nu/\lambda_{bulk}=30$ nm. The results of the fitting indicate an intermediate capture regime (α from 0.5 to 3); in these conditions, the indetermination intervals of the best-fit parameters L_+ and ν/λ_{bulk} are similar (ca. 20%). The quality of the fit is mediocre, but we wish to point out that: (a) the dispersion of the data reflects the true variability of microstructure of individual samples rather than the result of accidental measurement errors, and this variability is not included in our deterministic model; (b) a correction for taking into account positron trapping at the matrix-precipitate interface would certainly improve the fit in the region of large grain sizes.

In analogy to Fig. 6 regarding Al alloys, Fig. 10 illustrates the correlation between λ_A and intensity in Zn alloys, including STM and DTM model curves.

C. Fe-based alloys

Data on positron lifetimes in Fe-1.25 wt % C are given by Hidalgo, de Diego, and Ochando.[23,24] This material is a biphasic system, formed by a ferrite matrix containing cementite particles. The shortest lifetime resolved in the positron lifetime spectrum displays a systematic dependence on the ferrite grain size and on the temperature of the measurement; according to Refs. 23 and 24, it is to be interpreted as the mean life of positrons annihilated inside and at the surface of ferrite grains.

Following the above interpretation, we have fitted a DTM curve to the experimental points of Ref. 23. The result is shown in Fig. 11, where the lifetime labeled τ_1 in the original paper (but relabeled $\bar{\tau}$ in Fig. 11 to avoid changing the meaning of symbols used throughout this paper) is plotted vs the inverse ferrite grain size (the inverse size scale is the one chosen in the original work). The curve corresponds to the following values of fixed and adjustable parameters: $\lambda_{trap}/\lambda_{bulk}=0.64$, $\varepsilon=0.10$, $L_+=100$ nm, and $\nu/\lambda_{bulk}=100$ nm. However, excellent

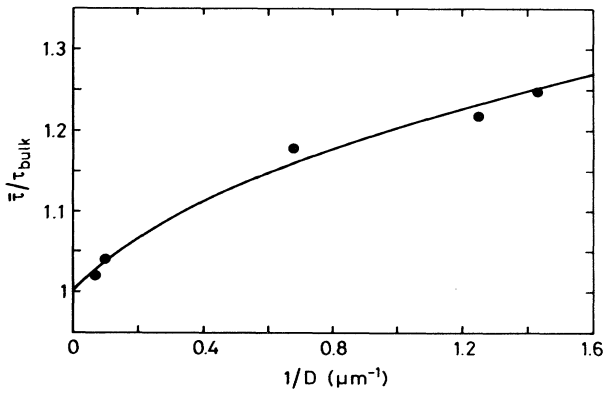

FIG. 11. Mean life $\bar{\tau}$ vs inverse grain size in the Fe-1.25 wt % C alloy. The experimental points are from Ref. 23, the curve is the DTM best fit.

fits can be obtained in a very large L_+ interval (90–400 nm), with modest adjustments of ν/λ_{bulk} (from 105 to 75 nm).

D. Pure metals

For completeness in our review of new and old results, we wish to recall that experimental evidence of positron trapping at grain boundaries was found for Be and Fe by Weisberg and Berko,[25] and for Cu by Lynn, Ure, and Byrne.[26] However, the available data are not sufficient for attempting a fit with DTM curves.

V. CONCLUSIONS

The first conclusion that one draws from the results of the previous section is that positron trapping at grain boundaries is a rather simple phenomenon, which can easily be incorporated within our present views on positron dynamics. The inconsistencies between experimental results and STM predictions mentioned in Refs. 16, 20, 21, and 27 are real, but we do not need to find a physical explanation for them, since the STM is a bad approximation when trapping is limited by transport. On the contrary, the curves calculated according to our simple version of the DTM fit the experimental points as nicely as one can expect in this type of experiment. Complications due to different species of traps,[21] or to the finite width of the intergrain disordered region,[20] do perhaps exist, but their effect remains hidden within the limits of the rather large statistical dispersion of the data.

The second point is that the determination of best-fit DTM curves provides quantitative estimates of two interesting physical parameters: the positron diffusion length L_+ and the specific trapping rate ν. However, since the relative importance of these two parameters in determining the result of the DTM calculation drastically changes when proceeding from the diffusion-controlled regime to the other extreme, it may occur that only one parameter (L_+ or ν) can be estimated with precision. In any case, it is crucial not to waste information: a fitting that takes into account intensities as well as lifetimes is always more discriminating than a fitting limited to only one of these variables, or to a single combination of them (e.g., mean life). The full use of the available data allowed us to reduce the indetermination interval of L_+ to ca. 5% in the most fortunate case (Al-based alloys). Clearly, these restricted error limits apply only for comparisons between data obtained with the same model and the same procedure. Some details of the model are important; for instance, if one assumes that the grains are cubic instead of spherical, the estimates of the diffusion lengths are reduced approximately by a factor of $\sqrt{3}$.

Nevertheless, it is interesting to compare the positron diffusivity values derived from our estimates of L_+ with the few available theoretical and experimental data for pure metals. Here are some numbers. For Al alloys, our value is $D_+ = 0.55 \pm 0.05$ cm^2/s; for pure Al at room temperature, we find in the literature the following values: 0.4 cm^2/s (theory[28]), 0.76 cm^2/s (from a transmission experiment[29]), 0.19–0.33 cm^2/s (from early beam experiments[30,31]), 1.3–2 cm^2/s (from recent beam experiments[32]). The scattering of the experimental values for Al may come from different assumptions in the data analysis and, most probably, the highest estimates are more accurate; if this is true, the difference from our result originates from the compositional disorder of the alloy. For the Zn-33 wt % Al, the DTM analysis gives 0.6 ± 0.2 cm^2/s, which is to be taken as a sort of average for the two phases of the system; the theoretical value for pure Zn is 0.5 cm^2/s. For ferrite in the Fe-C alloy the DTM analysis gives a diffusion coefficient in the interval 0.8–15 cm^2/s; for pure Fe, the results of a positron depolarization experiment[33] indicate $D_+ > 1$ cm^2/s.

We remark that the DTM estimates of the diffusivity are significantly smaller than the values obtained by the STM analysis. The comparison must be made under the same assumption for the shape of the grains; reporting all the data to the spherical geometry assumed in our model implies a multiplication by 3 of the values obtained for the cubic geometry. This gives the following STM values: 6 cm^2/s for Al alloys,[17] 1.8 cm^2/s for Zn alloys,[19] and 3 cm^2/s for the Fe-C alloy.[24]

Our determination of the trapping rate per unit specific surface ν leads to values ranging from ca. 0.2×10^5 cm s^{-1} (for Zn alloys) to ca. 3×10^5 cm s^{-1} (for Al alloys). The value regarding Al alloys is ca. 40% of the theoretical estimate for the Al-vacuum interface,[34] which can reasonably be considered as an upper limit for trapping at intergranular surfaces. We are not aware of surface specific trapping rates for Zn and Fe to be compared with our results. Considering that the specific trapping rates for defects of identical morphology in different metals are believed to coincide within an order of magnitude (see, for instance, estimates of the specific trapping rate for monovacancies in Al, Zn, and Fe in Refs. 34–37), the fairly large differences indicated by our results can probably be ascribed to dissimilar morphologies of the intergranular surfaces (e.g., number and extension of trapping sites per unit surface).

The starting point of this paper was the criticism of STM analysis in any case (extreme or intermediate) of diffusion-controlled positron trapping. We have shown in detail the differences between the full application of the diffusion approach and the STM approximation, but our study was limited to the specific case of trapping at grain boundaries. This is, however, not the only problem that has been treated with the approximation that we contest. Therefore we must end our paper with a word of caution, by noting that many currently accepted data on positron trapping are at best dubious. The same should be said for the field of positron and positronium chemical reactions, which are also partially or totally controlled by transport factors.

ACKNOWLEDGMENTS

This work was jointly supported by the Consejo Nacional de Investigaciones Científicas y Técnicas, Comisiòn de Investigaciones Científicas de la Provincia de Buenos Aires (República Argentina) and by the Ministero della Ricerca Scientifica e Tecnologica (Italia). Financial support was also provided by the International

Centre for Theoretical Physics, Trieste, Italia (A. Dupasquier) and by Fundaciòn Antorchas (A. Somoza).

APPENDIX: EXPERIMENTAL PROCEDURES

Our measurement of the dependence of annihilation characteristics on grain size in an Al-based alloy was performed using well-established techniques. Here are the important details of our experimental procedures.

1. Sample structure and preparation

Samples of commercial fine-grained superplastic Al-5 wt % Ca-5 wt % Zn sheet (2.4 mm thickness) were used. The microstructure of this material consists of a uniform dispersion of spheroidized $CaZnAl_3$ particles (about 20 vol %) in the aluminum matrix. According to Moore and Morris,[38] recrystallization in the conventional sense does not take place; the grain growth occurs when the boundaries are gradually released by second-phase particles that are disappearing during Ostwald ripening. The process accelerates with increasing temperatures.[18] In our case, grain coarsening was obtained with the following sequence of thermal treatments: (a) heating for 1 h at 823 K; (b) air cooling at room temperature; (c) isothermal annealing at $T_a = 773$ K, 798 K, or 863 K for times from 0 to 100 hs; (d) air cooling to room temperature. The effect of these treatments on the microstructure was examined by optical and electron microscopy, and the average size of the matrix grains and of the second-phase particles was determined by the intercept method. Before positron lifetime measurements, the samples were cleaned and etched with an aqueous solution of NaOH.

2. Positron lifetime measurements

The positron lifetime spectrometer was a fast coincidence system with a resolution of 260 ps. A source of 30 μCi ^{22}NaCl on a Kapton foil with a thickness of 7.5 μm was used in the usual sandwich geometry between two identical samples. The measurements were performed at room temperature. The lifetime spectra were analyzed with the PATFIT computer program.[39] After subtraction of the source contribution, a two-component analysis gave satisfactory fits in all cases. In our final analysis, the lifetime of the long-living component τ_B was fixed at 247 ps, which is the average value obtained from the constraint-free fitting. The results of this constrained analysis, averaged over four independent runs for each sample, are reported in Table I; the average experimental errors are of the order of 1 ps for the lifetime τ_A and 1% for the intensity I_B.

TABLE I. Positron lifetime measurements in Al-5 wt % Ca-5 wt % Zn; results of two-term fits with the constraint $\tau_B = 247$ ps.

Annealing temperature (K)	Average grain size (μm)	Lifetime τ_A (ps)	Intensity I_B (%)
773	0.84	155	43
	0.98	154	41
	1.07	155	40
	1.17	153	38
	1.21	158	36
	1.27	154	36
	1.31	158	34
	1.36	159	32
	1.39	156	31
	1.40	158	30
	1.43	154	31
	1.57	158	31
798	0.84	151	46
	1.00	162	45
	1.09	158	37
	1.15	153	37
	1.22	156	42
	1.23	153	38
	1.27	159	33
	1.31	155	35
	1.34	161	29
	1.40	155	34
	1.42	156	31
	1.48	159	33
	1.50	156	35
	1.53	156	31
	1.54	154	34
863	0.84	154	41
	1.26	157	33
	1.42	158	29
	1.58	158	30
	1.86	164	25
	2.12	163	26

[1] *Positrons in Solids,* edited by P. Hautojärvi (Springer, Berlin, Heidelberg, New York, 1979).
[2] *Positron Solid-State Physics,* edited by W. Brandt and A. Dupasquier (North-Holland, Amsterdam, New York, Oxford, 1983).
[3] W. Brandt and R. Paulin, Phys. Rev. B **5**, 2430 (1972).
[4] A. Seeger, J. Phys. F **3**, 248 (1973).
[5] W. Frank and A. Seeger, Appl. Phys. **3**, 61 (1974).
[6] W. Brandt, *Positron Solid-State Physics,* in Ref. 2, p. 1.
[7] W. Brandt, Appl. Phys. **5**, 1 (1974).
[8] C. H. Hodges, J. Phys. F **4**, L230 (1974).
[9] B. Bergersen and T. McMullen, Solid State Commun. **24**, 421 (1977).
[10] R. M. Nieminen, J. Laakkonen, P. Hautojärvi, and A. Vehanen, Phys. Rev. B **19**, 1397 (1979).
[11] W. Brandt, in *Positron Annihilation,* edited by A. T. Stewart and L. O. Roellig (Academic, London and New York, 1967), p. 155.
[12] D. C. Connors and R. N. West, Phys. Lett. **A30**, 24 (1969).
[13] B. Bergersen and M. J. Stott, Solid State Commun. **7**, 1203 (1969).
[14] J. Crank, in *The Mathematics of Diffusion* (Clarendon, Ox-

ford, 1956), p. 91.
[15]A. Somoza, R. Romero, and A. Dupasquier, Mater. Sci. Forum **105–110**, 1237 (1992).
[16]N. de Diego and C. Hidalgo, Philos. Mag. A **53**, 123 (1986).
[17]B. T. A. McKee, A. T. Stewart, L. Morris, and H. Sang, in *Positron Annihilation,* edited by R. R. Hasiguti and K. Fujiwara (Japan Institute of Metals, Aoba Aramaki, 1979), p. 169.
[18]R. Romero, S. P. Silvetti, and A. Somoza, Scr. Metall. Mater. **24**, 2225 (1990).
[19]B. T. A. McKee, G. J. C. Carpenter, J. F. Watters, and R. J. Schultz, Philos. Mag. **41**, 65 (1980).
[20]Yan Dong, L. Y. Xiong, and C. W. Lung, J. Phys.: Condens. Matter **3**, 3155 (1991).
[21]C. Hildago, N. de Diego, and F. Plazaola, Phys. Rev. B **31**, 6941 (1985).
[22]C. Hidalgo, N. de Diego, and M. A. Ochando, Solid State Commun. **49**, 611 (1984).
[23]C. Hidalgo and N. de Diego, Phys. Status Solidi A **80**, K145 (1983).
[24]C. Hidalgo, N. de Diego, and M. A. Ochando, Phys. Status Solidi A **83**, K93 (1984).
[25]H. Weisberg and S. Berko, Phys. Rev. **154**, 249 (1967).
[26]K. G. Lynn, R. Ure, and J. G. Byrne, Acta Metall. **22**, 1075 (1974).
[27]C. Hidalgo and N. de Diego, Appl. Phys. A **27**, 149 (1982).
[28]B. Bergersen, E. Pajanne, P. Kubica, M. J. Stott, and C. H. Hodges, Solid State Commun. **15**, 1377 (1974).
[29]A. P. Mills and R. J. Wilson, Phys. Rev. A **26**, 490 (1982).
[30]K. Lynn and H. Lutz, Phys. Rev. B **22**, 4143 (1980).
[31]K. G. Lynn and P. J. Schultz, Appl. Phys. A **38**, 293 (1985).
[32]E. Soininen, H. Huomo, P. A. Huttunen, J. Mäkinen, A. Vehanen, and P. Hautojärvi, Phys. Rev. B **41**, 6227 (1990).
[33]A. Seeger, J. Major, and F. Jaggy, in *Positron Annihilation,* edited by P. C. Jain, R. M. Singru, and K. P. Gopinathan (World Scientific, Singapore, 1985), p. 137.
[34]R. M. Nieminen and J. Laakkonen, Appl. Phys. **20**, 181 (1979).
[35]C. H. Hodges, Phys. Rev. Lett. **25**, 284 (1970).
[36]B. T. McKee, Phys. Rev. Lett. **28**, 358 (1972).
[37]A. Vehanen, P. Hautojärvi, J. Johansson, and J. Yli-Kauppila, Phys. Rev. B **25**, 762 (1982).
[38]D. M. Moore and L. R. Morris, Mater. Sci. Eng. **43**, 85 (1980).
[39]P. Kirkegaard, N. J. Pedersen, and M. Eldrup (unpublished).